Stiles–Crawford effect of the first kind: assessment of photoreceptor alignments following dark patching

Momoyo Kono [a,b], Jay M. Enoch [a,*], Elisabetta Strada [a], Paul Shih [a],
Ranjani Srinivasan [c], Vasudevan Lakshminarayanan [d], Wilbur Susilasate [a],
Andrew Graham [a]

[a] *School of Optometry (Mail Code 2020), University of California at Berkeley, Berkeley, CA 94720-2020, USA*
[b] *Department of Ophthalmology, Shiga University of Medical Science, Seta, Ohtsu, Shiga 520-2192, Japan*
[c] *Department of Biophysics, University of Illinois at Urbana-Champaign, Urbana, IL 61801, USA*
[d] *School of Optometry and Department of Physics and Astronomy, University of Missouri, Saint Louis, 8001 Natural Bridge Road, St. Louis, MO 63121-4499, USA*

Abstract

Properties of presumed mechanisms controlling photoreceptor alignments are partially defined. A phototropic mechanism normally dominates alignment, but do modest changes in orientations occur with dark patching? Here, new photopic Stiles–Crawford (SCE-I) determinations were made before patching (pre-patch), just after 8-days of dark-patching (post-patch), and 3 days after patch removal (recovery test). We tested at 0, 11 and 22° in the temporal retina of both eyes. Ten eyes of adult subjects were tested. SCE-I peak positions and Stile's parameter 'rho' were assessed. Dark-patching effects were small. Observations revealed meaningful corrective alignment overshoots with recovery in the light. Results suggest (1) the presence of multiple weak mechanisms affecting receptor alignments in the dark; (2) the phototropic mechanism to be dominant in the light; (3) the need for multiple test loci to be sampled in such studies, and (4) small changes in the SCE-I in the pupil plane can reflect meaningful events occurring at the retina. © 2000 Elsevier Science Ltd. All rights reserved.

Keywords: Retina; Stiles–Crawford effect of the first kind (directional sensitivity of the retina); Photoreceptor alignment (inferred); Effect(s) of dark patching

1. Introduction

The Stiles–Crawford function of the first kind (SCE-I), the 'directional sensitivity of the retina', assesses retinal responses to visible light entering different parts of the eye pupil Stiles and Crawford (1933), Enoch and Tobey (1981), Enoch and Lakshminarayanan (1991). From SCE-I data, orientation characteristics of assessed retinal receptors acting as fiber optic elements and waveguides may be inferred. In normal observers, photopic and scotopic peaks of the Stiles–Crawford function across the retina align approximately with the center of the entrance pupil of the eye. These responses

are very stable over time (e.g. Rynders, Grosvenor, & Enoch, 1995). In rod- and cone-dominant vertebrate species, central pupil-pointing by photoreceptors located across the retina was demonstrated histologically by Laties and co-workers (see Enoch & Tobey).

Receptors are subject to strains and stresses throughout life (Enoch & Tobey, 1981; Enoch & Lakshminarayanan, 1991). These are associated with accommodation, saccades (Westheimer, 1969), gravitational forces, a variety of trans-retinal tractional strains [scars, colobomas, twisted-disk syndromes (including myopia), dystrophic anomalies, etc.], forces associated with transfers of molecular constituents across the RPE-neural retinal interface during life, and modifications and repairs of receptors and associated tissues in response to insults. The stability of the SCE-I over many years, and the near consistent alignment of pho-

* Corresponding author. Tel.: +1-510-6429694; fax: +1-510-6435109.

E-mail address: jmenoch@socrates.berkeley.edu (J.M. Enoch).

toreceptors with a locus near the center of the eye pupil across the retina, contribute to an argument for the presence of an active and dominant photoreceptor alignment system (Bonds & MacLeod, 1978; Applegate & Bonds, 1981; Enoch & Birch, 1981). This argument has been tested by tracking the photopic SCE-I function in an eye wearing a displaced center contact lens (Enoch & Birch), and, in another study, by tracking the SCE-I in an eye with a displaced pupil center caused by a prior disorder, and determining the change in SCE-I when this eye was dilated for a period of several days to reveal a more normal/centered circular pupillary shape (Bonds & MacLeod, Applegate & Bonds, see also note added in Pro B). In these experiments, the peak of the SCE-I moved within days towards the center of the redefined pupil aperture. And, recovery to original status was carefully tracked after the experiment.

For maximum information capture from the environment, it is important to match the limiting apertures of photoreceptor waveguides to the eye pupil aperture (Enoch, 1972a; Enoch & Tobey, 1981; Enoch & Lakshminarayanan, 1991). Added factors help reduce stray light noise in the eye and optimize the retinal image (Enoch and Tobey, Enoch and Lakshminarayanan).

In the presence of certain retinal anomalies, such as retinal detachments, measured SCE-I functions are greatly disturbed. In many cases, following recovery, the SCE-I recovers essentially normal function. Such findings also suggest the presence of an active alignment system. From studies of patients with ocular disorders (e.g. Campos, Bedell, Enoch, & Fitzgerald, 1978), we infer that alignment is controlled locally in the retina (also see note added in Proof A). The RPE plays a key role in maintaining receptor alignments, because neurosensory retinal detachments can result in sustained photoreceptor mis-alignments, and reattachment of retinal receptors to the underlying RPE often results in recovery of alignments (Enoch & Tobey, 1981; Enoch & Lakshminarayanan, 1991). Initial alignment apparently is established in utero (the work of Laties, see Enoch, 1972a, Enoch & Tobey,). Chaitin and Burnside (1989) have demonstrated the presence of actin filaments in inner and outer segments of photoreceptors of Pinfish and rat. At least Pinfish are known to exhibit light/dark driven extensions and contractions.

From human displaced pupil aperture studies by Enoch and Birch (1981), and more recent studies of snake-eye receptor alignments following a laser burn (see e.g. Zwick, Elliott, Schuschereba, Lund, & Stuck, 1997; Zwick, Elliott, Li, Akers, Edsall, & Stuck, 1999); we have learned that receptors can vary their orientations in the retina in a wave-like or a spreading manner expanding from a defined reference or centrum. In more profound disorders, this orderly structure may be permanently disturbed.

In summary, there is probably a phototropic mechanism, it is capable of local control, and the phototropic response mechanism is robust, e.g. the SCE-I does not 'come apart' during sleep. We still do not understand how alignments are precisely maintained, nor many factors contributing to feedback controls of this alignment system. And it remains unclear what happens when the phototropic signal is withdrawn for an extended period of time? In this study, we re-examined this issue. Subjects were occluded monocularly for a period of dark-patching lasting 8 days.

1.1. Development of the working hypothesis

Previously, we studied three eyes (one not reported) where alignment was directed towards the center-of-the-retinal-sphere rather than towards the center-of-the-eye-pupil (Bedell & Enoch, 1980; Enoch, Eisner, & Bedell, 1982; Enoch, Lakshminarayanan, & Yamade, 1986; Lakshminarayanan, Enoch, & Yamade, 1987). In these three eyes, the phototropic system was not dominant. Current subjects did not exhibit this property. However, from studies of such cases, one may infer that a second system, perhaps driven by molecular exchanges occurring during life, dominated in those unusual eyes (e.g. Enoch & Lakshminarayanan, 1991). In these few cases, trans-retinal receptor alignment was roughly perpendicular to the retina. Note, for both near center-of-the-pupil pointing (normal), and center-of-the-retinal-sphere pointing cases (abnormal), there should be little difference in SCE-I peak location at the posterior pole of the eye, because of the near common alignment of the exit pupil of the eye, and the center of the retinal sphere with the central retinal area. Thus, in addition to testing at fixation, here we tested retinal loci away from the posterior pole of the eye.

When the problem assessed in this paper was first considered (e.g. Enoch & Birch, 1981; Enoch, Birch, & Birch, 1979; Enoch, Birch, Birch, & Benedetto, 1980), JME and his then co-workers made errors. Eisner first noted a non-consistency (not published), Applegate et al., and later, Enoch et al., noted the discrepancy, and this has since been rectified in the literature (Applegate, Adams, Bradley, & Eisner, 1986; Enoch et al., 1987). The large effects which were described earlier with dark-patching were not found on retest. JME took full responsibility for errors made (Enoch & Birch, 1985; Enoch et al., 1987). Here we ask, 'are small effects detectable with dark-patching'?

Working hypothesis, assume there are three dominant alignment mechanisms, (1) a phototropic mechanism; (2) a metabolically active mechanism acting approximately perpendicular to the retinal wall, and (3) tractional strains affecting photoreceptor alignments. Tractional effects were reduced by pre-selecting subjects such that no evidence of marked trans-retinal tractional

strains was noted in retinal areas sampled. Testing was not limited to subjects with perfectly centered SCE-I peaks. Rather more extreme decentrations, and consistent non-central pupillary biases in centrations were a reason for exclusion. We then tested at fixation, at 11° in the nasal visual field (temporal retina), and at 22° in the nasal visual field. We avoided testing loci near the blind spot, because tractional effects are rather commonly encountered between the point of fixation and the blind spot (e.g. JME's eye in Enoch & Birch, 1981). One cannot assume homogeneity of photoreceptor alignment (finely assessed) trans-retinally (e.g. Enoch & Hope, 1972; Enoch & Birch, 1981; Enoch & Tobey, 1981; Enoch & Lakshminarayanan, 1991).

If the working hypothesis is correct, at fixation we should see little change in alignment with dark-patching. And if response in the dark shifted towards a control system aligned with the center of the retinal sphere, there should be increasing differences in SCE-I peak locations at 11° and more at 22° between the pre-test and the post-patching tests and the shifts occurring should be nasally-directed (see model, Enoch & Hope, 1972).

Data were sampled multiply pre-test after extended initial training. Pre-test training sessions provided information relative to approximate peak locations as well as the curvatures of the SCE-I functions, and helped define best points to sample in the entrance pupil of the eye in order to provide optimal assessments of SCE-I peak and curvature determinations during the studies reported here. Multiple pre-patch determinations provided means of determining observer reliability at each test locus. After extended patching, each retinal locus was tested promptly. This was repeated again after 3 days of recovery without dark patching (Applegate & Bonds, 1981; Enoch & Birch, 1981; Enoch & Tobey, 1981; Enoch & Lakshminarayanan, 1991). SCE-I peak locations and curvatures of the photopic SCE-I parabolas (rho determinations) were made and difference functions were determined.

We approached the statistical analysis broadly, because there are many variables to consider. We asked, was the peak of the SCE-I detectably different just after patching when compared with the pre-patching status? If so, were biases present, i.e. did the peaks tend to translate nasally or temporally? And did the SCE-I functions become either somewhat flatter or steeper after patching, and if so, were biases towards flatness or steepness caused by dark-patching? All issues were phrased to allow a test of the null hypothesis.

2. Apparatus and methods

The apparatus is the same (with modest modifications updating the device) as reported in Enoch and Hope (1972). Main design changes were (1) substitution of an IR CCTV for the image converter, and (2) a VDT for monitoring iris size, proper focus in the plane of the entrance pupil of the eye, and pupil and stimulus positions during testing (as well as a means to record eye movements, contact lens displacements, etc.). A low power HeNe laser coupled with a precision height gauge, precision levels, a permanent array of set and localized pinholes, as well as precision pentaprisms were used for fine alignment of the optical system.

Stile's field sensitivity increment threshold technique was employed to measure the SCE-I (Enoch & Hope, 1972; Enoch & Birch, 1985). A beam of light, 0.3 mm diameter, in the entrance pupil of the eye was directed at the defined retinal locus. It was flashed at 150 ms once each second, and subtended 0.5° in the visual field. The flashing light spot was superimposed upon the center of a steady-state background having a 4.0° diameter field. The pupillary trace (beam) of the background field was translated in the entrance pupil of the observer's (dilated) pupillary aperture in order to measure the horizontal SCE-I function. All measurements were obtained by testing within the linear portion of the observer's Weber function (Enoch, 1972b, Enoch & Hope). Weber functions were determined for each subject at each test locus prior to SCE-I determinations. The background field had a luminance of 192 cd m^{-2} in the plane of the entrance pupil of the eye (and a beam diameter of 0.3 mm).

All calibrations of luminance were conducted using a Spectra Physics Pritchard Photometer fitted with a $10 \times$ microscopic objective. In each case, the field area assessed for calibrations (luminance, color filters, neutral density filters) was the central portion of the 0.3 mm exit pupil of the instrument. When determining the effect of translating these small beams in the entrance pupil of the eye, a Leeds and Northrop integrating sphere was employed. The output of this unit was measured through a side-window.

Both fields entered the dilated eye pupil using Maxwellian view optics. Testing was photopic as revealed by separate increment threshold studies associated with Weber function determinations. To minimize SCE-II (hue and saturation-related) effects (Enoch, 1972b; Enoch & Stiles, 1961), a Wratten 23A filter (orange–red pass band) was used during all testing. This was used in concert with CIE Illuminant A (6 V, 18 A ribbon tungsten lamp filament lamp; General Electric) operated at 14 A. The latter setting provided good stability in our system. This provided a modest red bias to the output when one compares use of this same bulb as Standard Illuminant A. The entry position of the background field beam at the pupil was altered in discrete programmed steps along the horizontal pupillary diameter. Location of the translated beam was limited to ± 3.0 mm from the peak of the SCE-I

measured function (estimated during training trials, Stiles, 1937; Enoch, 1972b; Enoch and Stiles, 1961; Lakshminarayanan and Enoch, 1985). Calibrated radiance was not affected by the translation of either beam in the entrance pupil, nor the careful field stop corrections required when the background field was translated. The field stop, associated with the background field, was recentered in the eye pupil after each translation of the beam.

The sharply focused test field beam was located at the geometric center of the eye pupil. The observer was held in place with a bite bar and a head rest. In addition, the position of the dilated pupil and locations of the test and background field beams in the entrance pupil of the eye were monitored (and corrected as needed) continuously with the help of the IR CCTV system. Our ability to control the position of the observer's eye pupil during SCE data runs was ± 0.1 mm. Observers were provided with 3 min of light adaptation prior to testing when the background test beam was shifted or when any change in test conditions occurred. Subjects remained on the bite bar throughout the SCE-I test. The increment threshold was determined by adjusting the luminance of the small field flashing test beam centered in the entrance pupil of the eye. We measured both from seeing to just non-seeing (data set A), and from non-seeing to just detection (data set B). Dial readings from a precision potentiometer were measured. The angular position of a balanced Eastman Kodak 2.0 log unit neutral density wedge was read.

Six normal White and Asian subjects, M and F (age 24–35 years) were examined. Four were tested in both eyes, two in one eye (right eye). Subjects 'P' and 'w' chose not to continue the experiment after completing the test on the one eye. Reference data on subjects are presented in Table 1.

Informed consent was obtained prior to testing. Exclusion criteria were, best corrected VA of less than 20/20 in eyes tested; evidence of, or history of meaningful ocular diseases or abnormalities (including narrow anterior chamber angles); high refractive errors; evidence of consistent traction affecting meaningfully the SCE-I at or near retinal loci sampled (see above); dental appliances which might have been adversely affected by molding or use of a bite bar; and a failure by the subject to provide reliable data after extended training.

Visual corrections were obtained with contact lenses when required (Table 1). The pupil was dilated with 1% tropicamide and 2.5% phenylephrine hydrochloride. Generally, two drops of each agent were used, and the dilation was maintained at about 8 mm diameter throughout. After initial training, pre-patch data sets were taken at the three selected test loci in each eye. A minimum of two normal sets of SCE-I data (post-training) were obtained pre-patch at each test site. Testing was limited to the horizontal meridian in the entrance pupil of the eye tested.

Solid plastic black patches with foam plastic spacers were used (Franel Optical Supply Corp., Maitland, FL). These were worn continuously during patching. No light was visible through the occluders and no pressure was placed on the eye. A non-skin contacting nor adherent 'skirt-like extension' (made of black tape and dense black felt) enlarged the boundary of the occluder by about 1 in. This provided darkness and air exchange. At the end of 8 days the occluder was removed in the darkened laboratory, and the subject was tested at the three test loci in the order, 22° nasal visual field, at fixation, and at 11° nasal visual field. And each eye of each subject was examined carefully to determine if anomalous changes had occurred to/in the eye (none found). After 3 days, an added set of recovery data were obtained at the same three test loci.

3. Results

Data were processed separately on repeated occasions at different sites. The first of the data reviews was conducted shortly after completion of each data set. This determined whether a given data set was acceptable for inclusion in the larger sample. That is, did excessive outlying points exist in a data set (very rare), was there evidence for change in criterion of psychophysical judgements during the test session (reasonably rare, diminished by training), did the subject experience or express discomfort or was there an interruption during testing (any cause), etc.? If such a judgement was made, the entire SCE-I test was repeated after a suitable rest period and these new data were used for analysis. If a data set was 'atypical', but did not justify rejection for cause, added data sets were taken in order to increase the data base and to obtain a sounder estimate of outcomes (a maximum of four data sets were included in a single estimate).

Table 1
Subject sex, age, refraction and snellen acuity

Subjects	Sex	Age	Refraction	VA
K	F	35	OD, -0.25	20/15
			OS, PLANO $= -0.25 \times 180°$	20/20
E	F	30	OD, PLANO $= -0.50 \times 45°$	20/20
			OS, -0.50	20/20
B	F	30	OD, $+0.25 = -0.25 \times 90°$	20/15
			OS, PLANO $= -0.50 \times 45°$	20/15
W	M	24	OD, -5.50[a]	20/15
			OS, -4.50	20/20
P	M	24	OD, $-6.50 = -0.25 \times 5°$[a]	20/15
			OS, $-6.50 = -0.25 \times 38°$	20/15
V	F	24	OD, PLANO	20/15
			OS, PLANO	20/15

[a] Single eye tested.

In each subset of data, seven repetitions of each increment threshold judgement were obtained. Seeing to non-seeing (data set A), and non-seeing to seeing (data set B) were tallied separately. High and low readings were dropped immediately from each of these two data sets.

In an initial 'in house' laboratory analysis, means of the A and B data sets (A and B) were merged. During a test 'run', the order of testing was as follows. Initially, for determination 1, the Maxwellian beam trace of the background field in the entrance pupil of the eye was located centrally in the pupil (X and Y axes = 0 mm). Increment thresholds were determined. This data set was designated 0_1; then a horizontal displacement of $\pm X_1$ was made and the increment thresholds determined; then 0_2; then $\pm X_2$; followed by 0_3, ...; and finally, 0_n. After individual increment threshold means and S.D. were determined, the means of 0_1 and 0_2 were determined, they were averaged to provide the mean value $0_{(1,2)}$, etc. The ratio of the increment threshold at X_1 was taken relative to the determined mean value of the increment threshold, $0_{(1,2)}$; X_2 relative to $0_{(2,3)}$, ...; $X_{(n-1)}$ relative to $0_{[(n-1),n]}$. These relative values of the increment threshold were plotted, and SCE-I peak location (X_{max}) and rho (ρ; estimate of curvature of the parabola) for each set of data were determined by comparisons with templates. All values determined at $X = Y = 0$ were set equal to 1.0 or $\log_{10} X = 0.0$. The S.D. of values for the several 0 settings (0_1, ..., 0_n) were plotted as an indicator of reliability of performance for each SCE-I data set.

The statisticians maintained separate the two data subsets A and B, as well as data for each eye. All data were taken as provided (less the highs and lows, and the small number of designated unambiguous individual outlier data points (for this very large test series, nine points); the latter were deleted 'up front'). The SCE-I peaks and rhos for each data set were determined. All relative sensitivity values were estimated relative to the determined peak location of the individual SCE-I data set, instead of pupil center location ($0_{(X,Y)}$-used in the initial or 'quick-on-site' analysis conducted in the laboratory).

Sample data, sample data sets and figures are shown. The entire data set and all figures will be maintained for a period of several years at the following http://psiphi.umsl.edu/vengu/.

Arbitrarily, data sets obtained from subject b (Table 1) are presented here. Table 2 provides the basic computational data set for this subject; data sets A and B are separated. A four symbol code was applied to each subset of data. (1) The first letter refers to the subject tested [b]; (2) the second letter refers to a test of the right (d) or left (s) eye; (3) the first number refers to pre-, post-, and recovery testing; i.e. #1 = control, normal, or pre-dark-patch test data, #2 = (prompt)

post-dark-patch data testing, and #3 = recovery phase (72 h after patch removal) testing; and symbol (4) addresses retinal locus tested, i.e. #1 = 0° or fixation, #2 = 11°, and #3 = 22° in the nasal visual field. For example, refer to Table 2, Data set A (seeing to non-seeing); bd11 = subject b, right eye, pre-patch-test at the fixation point. In these tables, all data for a given test condition are combined (e.g. bd11 included three SCE-I test sets).

In Table 2 'peak' refers to the value of $\log_{10} \eta'/\eta'_{max}$ at the SCE-I peak location, X_{max}. These values deviate slightly from 1.0 in log units. Sig-Peak indicates the S.D. of this value in log units. Curvature refers to rho (ρ) values which are always negative. Sig-curv is the S.D. of the estimate of rho (for added details see notes below).

X_{max} in mm, is expressed as (N)asal or (T)emporal in the horizontal meridian of the entrance pupil of the eye. It is plotted linearly on the abscissa in figures. For ease of comparisons between eyes and data sets, all values Nasal for right and left eyes are plotted or designated to the left, and all values temporal are designated to the right. Sig-X_{max} in mm is the S.D. of the location of the peak of the measured SCE-I function. Again, only the horizontal pupillary meridian was tested. χ^2-Values are listed.

In this study, we are interested in differences in the SCE-I resulting from dark patching, as well as recovery from this test condition. In Tables 3 and 4 differences in X_{max} and rho are presented. In both tables, file code refers to the first two letters of the four symbol designator used in Table 2, and post–pre is the difference in location of the peak of the SCE-I function determined just after patching relative to the peak value obtained before patching. Addressing the first line of Table 3, data set A, 0°, right eye, post–pre for bd is the equivalent of [bd21 − bd11] = 0.0548 T or a shift temporally of X_{max} in the entrance pupil of the eye by 0.0548 mm from the original pre-patch determination (see Fig. 1). Staying with measures of X_{max}, subject bd, data set A, at 0°, the rec–pre value is equivalent to [bd31 − bd11] = 0.0804 N or a nasal shift with recovery relative to the pre-patch measurement (see Fig. 2); and for the same subject, rec–post at 0° is equivalent to [bd31 − bd21] = 0.1352N or a nasal shift associated with recovery relative to the SCE-I peak location determined just after patch removal (see Fig. 3).

Table 4 addresses differences in the values of ρ with test condition. This table is organized similarly to that seen in Table 3. A positive change implies the SCE-I became flatter, and a negative change signifies an increase in ρ, or a steepening of the curvature of the parabola fitted to the SCE-I function. Thus, again for data set A, right eye, 0°, subject b, post–pre, a value of [bd21 − bd11] = −0.02620 (ρ units) is recorded. In other words, just after patching, the SCE-I at this

Table 2
Parts a and b data sets of subject b[a]

File code	Peak	Sig-peak	Curvature	Sig-curv	X_{max}	Sig-X_{max}	χ^2
Data A							
bd11	0.98727	0.03150	−0.02911	0.01257	0.26335N	0.28403	0.8111
bd12	0.99825	0.01416	−0.05550	0.00756	0.26182N	0.07497	2.0817
bd13	0.95209	0.03536	−0.03052	0.02143	0.10039N	0.32009	1.2277
bd21	0.97846	0.01790	−0.05531	0.00917	0.2086N	0.08356	1.4413
bd22	0.96239	0.01894	−0.06199	0.00987	0.26935N	0.08043	1.9831
bd23	0.98792	0.01856	−0.04460	0.01009	0.34985N	0.12516	3.4869
bd31	1.00181	0.02429	−0.01509	0.01175	0.34377N	0.44755	0.2385
bd32	1.01660	0.01731	−0.05778	0.00853	0.27304N	0.08050	1.1025
bd33	0.97553	0.02867	−0.04773	0.01312	0.06748N	0.11109	0.9092
bs11	0.98931	0.02760	−0.03046	0.01156	0.33153N	0.24855	1.3431
bs12	0.95694	0.03697	−0.05201	0.01905	0.25278N	0.18401	1.5846
bs13	0.96475	0.04929	−0.04584	0.02659	0.06964T	0.26894	0.2666
bs21	1.00120	0.02154	−0.04472	0.00948	0.49109N	0.15077	6.3590
bs22	0.94941	0.02786	−0.05513	0.02118	0.26916N	0.17787	2.6671
bs23	0.97380	0.02673	−0.03365	0.01411	0.05898T	0.20756	0.8337
bs31	0.99709	0.02078	−0.04318	0.00909	0.46003N	0.13903	0.4415
bs32	0.98047	0.03194	−0.05493	0.02032	0.12807N	0.16842	0.5950
bs33	0.95035	0.02800	−0.02655	0.01591	0.19183N	0.28661	2.0929
Data B							
bd11	0.97679	0.03307	−0.02677	0.01312	0.17614N	0.29315	1.2231
bd12	0.99158	0.02502	−0.05780	0.01305	0.31172N	0.13036	0.2381
bd13	0.96769	0.03544	−0.05685	0.01977	0.05815N	0.16244	0.6991
bd21	0.97470	0.02437	−0.05168	0.01264	0.20634N	0.12245	2.7541
bd22	0.96995	0.02010	−0.06208	0.01031	0.30442N	0.08550	5.9499
bd23	0.97509	0.03023	−0.04970	0.01480	0.21838N	0.14235	0.8586
bd31	0.98930	0.02426	−0.04004	0.01040	0.03376T	0.11765	1.6293
bd32	0.98114	0.03167	−0.05757	0.01644	0.2695N	0.14347	1.7344
bd33	0.94396	0.03141	−0.04662	0.01650	0.09803N	0.15138	3.4972
bs11	0.99261	0.03025	−0.03959	0.01278	0.60546N	0.28319	2.6155
bs12	0.96375	0.03483	−0.06924	0.01660	0.20909N	0.11290	0.5648
bs13	0.96673	0.04908	−0.06383	0.02624	0.05317T	0.18118	0.4835
bs21	0.98752	0.02766	−0.05337	0.01166	0.60201N	0.17808	3.2979
bs22	0.96069	0.02823	−0.08413	0.01883	0.30293N	0.11418	1.6073
bs23	0.96182	0.03362	−0.05229	0.01814	0.21595N	0.17121	2.6835
bs31	1.01742	0.02047	−0.06475	0.00842	0.42781N	0.08322	4.9830
bs32	0.97955	0.03229	−0.07389	0.02304	0.24799N	0.16816	0.8898
bs33	0.97026	0.04241	−0.05374	0.01999	0.31688N	0.19242	0.6538

[a] Data set A refers to seeing to just non-seeing increment threshold SCE-I data. Data set B refers to non-seeing to just seeing increment threshold SCE-I data. See text for designations of columns in these two data sets.

location has a −0.02620 steeper value of rho than the SCE-I value measured prior to patching etc.

Figs. 1–3 provide a small number of sample data sets for Subject b: these show bd21 versus bd11 (Fig. 1), bd31 versus bd11 (Fig. 2), and bd31versus bd21 (Fig. 3). Each of these figures shows the data points included in each analysis, the best fitting curves, the location of the peaks (V and V), and the confidence limits for each data set. Here, the 95% confidence intervals are shown. Data are separated into sets A and B. The abscissa is in mm in the entrance pupil of the eye, nasal and temporal. For each pair of data sets, there were also plotted 99% confidence intervals; these are not included in the samples presented (see URL). The SCE-I data sets appear flatter than usual plots of SCE-I. This is a detail associated with NET transmission of data between

laboratories, and the desire to include two data sets (A and B) in each figure and to retain sufficient detail for printing and reproduction. These data are not atypical relative to other SCE-I data sets. All measured changes in values of X_{max} and rho in this dark patching experiment are small.

4. Statistical analysis I

These data were analyzed as a tri-level split-plot design with repeated measures at the lowest split level. Response variables were (ρ) curvature of the parabola (Stiles' equation) fitted to SCE-I functions (Stiles, 1937; Lakshminarayanan & Enoch, 1985), and X_{max}, the x-coordinate in the entrance pupil of the eye of the

maximum of SCE-I. The analyses were done using PROC MIXED in a SAS software package (Littell, Milliken, Stroup, & Wolfinger, 1996). The models were based on subjects as blocks, eyes as whole plot treatment, test condition (pre-patch, post-patch, and recovery) as first split level, A and B data sets as second split level, and retinal test loci (0, 11, and 22° in the temporal retina) the third level. Retinal test loci were treated as having a covariant structure; the measurements of ρ had a compound symmetry structure, and X_{max} had a Toeplitz or unstructured structure.

In this first analysis, two different statistical models were fitted for the two response variables; (1) X_{max} and (2) ρ or curvature of the parabola. A mixed model was used for both variables in which both fixed and random components were included. It was assumed that the errors associated with the different test loci had a covariant structure. The fixed effects were (a) test conditions, (b) eyes, * A and B data sets, and (d) retinal test loci. The random effects were (a) subjects, (b) subject*eyes, * subject*eyes*(test conditions), and (d)

subject*eyes*(test conditions)*(A and B data sets). The split plot design was used in modeling, which divides the different effects in a hierarchical fashion. The F statistic was calculated to verify or negate the null hypothesis, i.e. to test which effects were significant. The corresponding probability values are listed in tables, which follow.

All possible interactions between the fixed effect variables were tested, and thereby were retained or discarded in the final model based on whether these effects were significant or not. It was found that no significant interactions were present between the fixed effects in the model for rho. The model for X_{max} had only one significant interaction term, i.e. eye*(retinal test locus), which is therefore included in the final model. Finally, the analyses were performed for both weighted (weighted by the inverse of the variances obtained from the quadratic fits to the SCE-I data sets) and unweighted response variables.

As can be seen from Table 5, part 1, ρ, there is a significant difference in curvature between A and B

Table 3
Differences determined in SCE-I peak locations (X_{max}) between (1) post-dark-patching (immediate measurements) and pre-dark-patching (control) data sets (post–pre) (2) recovery data (72 h) and pre-dark-patching data sets (rec–pre) (3) recovery and post-dark-patching data sets (rec–post)[a]

File code	0°			11°			22°		
	Post–pre	Rec–pre	Rec–post	Post–pre	Rec–pre	Rec–post	Post–pre	Rec–pre	Rec–post
Data A right eye									
bd	0.0548 T	0.0804 N	0.1352 N	0.0075 N	0.0112 N	0.0037 N	0.2495 N	0.0329 T	0.2824 T
ed	0.1022 T	0.2078 N	0.3101 N	0.0426 T	0.0370 N	0.0796 N	0.0708 T	0.0930 T	0.0223 T
kd	0.0544 N	0.0369 T	0.0913 T	0.1567 N	0.2009 N	0.0442 N	0.1461 N	0.0056 T	0.1517 T
vd	0.1222 N	0.4274 T	0.5497 T	0.1940 N	0.0373 N	0.1566 T	0.0479 T	0.1613 T	0.1134 T
pd	0.0703 N	0.1676 N	0.0972 N	0.23929 T	0.0639 T	0.1689 N	0.1374 N	0.0358 N	0.1016 T
wd	0.3080 T	0.3374 T	0.0294 T	0.0628 N	0.0107 T	0.0735 T	0.1186 T	0.0323 N	0.1509 N
Data B right eye									
bd	0.0302 N	0.2099 T	0.2401 T	0.0073 T	0.0422 T	0.0349 T	0.1602 N	0.399 N	0.1203 T
ed	0.1172 T	0.0571 N	0.1743 N	0.0309 N	0.0997 N	0.0688 N	0.1252 T	0.1150 T	0.0103 N
kd	0.0056 N	0.2430 N	0.2375 N	0.0697 N	0.0306 N	0.0392 T	0.1273 N	0.2487 T	0.3760 T
vd	0.0624 T	0.4255 T	0.3631 T	0.2001 N	0.1391 N	0.0610 T	0.1034 T	0.1039 T	0.0005 T
pd	0.0080 N	0.1883 N	0.1803 N	0.3732 T	0.1904 T	0.1827 N	0.1073 T	0.1800 T	0.0727 T
wd	0.0356 T	0.1968 T	0.1612 T	0.1268 N	0.0752 N	0.0516 T	0.0500 T	0.2060 N	0.2560 N
Data A left eye									
bs	0.1596 N	0.1285 N	0.0311 T	0.0164 N	0.1247 T	0.1411 T	0.0107 N	0.2615 N	0.2508 N
es	0.2282 T	0.2238 T	0.0044 N	0.1727 T	0.2004 T	0.0277 T	0.3184 N	0.0002 T	0.3186 T
ks	0.2426 N	0.1182 T	0.3608 T	0.1082 N	0.0360 T	0.1441 T	0.0107 T	0.2444 N	0.2551 N
vs	0.0139 T	0.0758 N	0.0897 N	0.2673 N	0.0654 N	0.3327 T	0.0880 T	0.2960 N	0.3840 N
Data B left eye									
bs	0.0034 T	0.1777 T	0.1742 T	0.0938 N	0.0389 N	0.0549 N	0.2691 N	0.3700 N	0.1009 N
es	0.1715 T	0.1564 T	0.0150 N	0.1732 T	0.0483 T	0.1249 N	0.1111 N	0.0593 T	0.1704 T
ks	0.0738 N	0.1252 T	0.1990 T	0.1773 N	0.0927 N	0.0846 T	0.1637 N	0.3182 N	0.1545 N
vs	0.0443 T	0.1125 N	0.1569 N	0.1553 N	0.0449 T	0.2002 T	0.0010 T	0.2103 N	0.2113 N

[a] Data are provided for the six subjects for data sets a and b; right (d) and left (s) eyes; and retinal test locations; fixation or 0, 11, and 22° in the temporal retina. N, a measured shift of the SCE-I peak in the nasal direction in the entrance pupil of the tested eye for the defined difference in the two SCE-I data sets; T, a shift of the SCE-I peak in the temporal direction in the entrance pupil of the eye for comparable measurements. The following tables show the differences in the location of the peak position (X_{max}) between various test conditions. For example, post–pre gives the difference in X_{max} for the Stiles–Crawford function after patch removal and before patching. The 'N' or 'T' indicates whether the X_{max} values have shifted in a nasal or temporal direction, respectively.

Table 4

Differences determined in SCE-I rho (ρ), the curvature of the parabola defined in stiles' SCE-I equation, between (1) post-dark-patching (immediate measurements) and pre-dark-patching (control) data sets (post–pre) (2) recovery data (72 h) and pre-dark-patching data sets (rec–pre) (3) recovery and post-dark-patching data sets (rec–post)[a]

File code	0°			11°			22°		
	Post–pre	Rec–pre	Rec–post	Post–pre	Rec–pre	Rec–post	Post–pre	Rec–pre	Rec–post
Data A right eye									
bd	−0.02620	0.01402	0.04022	−0.00649	−0.00178	0.00471	−0.01408	−0.01721	−0.00313
ed	0.00410	0.00928	0.00518	−0.01068	−0.05677	−0.04609	0.00539	−0.01670	−0.02209
kd	−0.01150	0.00032	0.01182	0.00157	0.00944	0.00787	0.00852	0.00640	−0.00212
vd	0.01365	−0.01351	−0.02716	−0.00434	−0.00483	−0.00049	−0.04673	−0.01898	0.02775
pd	−0.00378	−0.05161	−0.04783	−0.01019	−0.00559	0.00460	−0.01145	0.01161	0.02306
wd	−0.00173	−0.00991	−0.00818	−0.00013	−0.01685	0.01672	−0.00648	−0.00899	−0.00251
Data B right eye									
bd	−0.02491	−0.01327	0.01164	−0.00428	0.00023	0.00451	0.00715	0.01023	0.00308
ed	0.00404	0.01237	0.00833	0.00170	−0.04286	−0.04456	−0.00627	−0.02980	−0.02353
kd	−0.01160	0.01900	0.03060	0.00070	−0.00401	−0.00471	0.00229	−0.00318	−0.00547
vd	0.01431	−0.01781	−0.03212	0.00500	0.00401	−0.00099	−0.01836	−0.03083	−0.01247
pd	0.02308	−0.05122	−0.07430	−0.02014	−0.01093	0.00921	−0.00645	−0.00066	0.00579
wd	−0.01546	−0.01915	−0.00369	0.01045	−0.00474	−0.01519	−0.00262	−0.01304	−0.01042
Data A left eye									
bs	−0.01426	−0.01272	0.00154	−0.00312	−0.00292	0.00020	0.01219	0.01929	0.00710
es	−0.01659	−0.02654	−0.00995	0.00706	0.01655	0.00949	0.02367	0.01374	−0.00993
ks	−0.00111	−0.02595	−0.02484	−0.00154	−0.00730	−0.00576	−0.01181	0.01049	0.02230
vs	0.00125	−0.01678	−0.01803	0.01368	0.00017	−0.01351	−0.00885	−0.03178	−0.02293
Data B left eye									
bs	−0.01378	−0.02516	−0.01138	−0.01489	−0.00465	0.01024	0.01154	0.01009	−0.00145
es	−0.02028	−0.02264	−0.00236	0.00323	0.02262	0.01939	−0.00054	−0.00373	−0.00319
ks	−0.01355	−0.01866	−0.00511	0.01260	0.01455	0.00195	0.00810	0.02660	0.01850
vs	0.00017	−0.01886	−0.01903	0.01885	0.00614	−0.01271	−0.02768	−0.03689	−0.00921

[a] Data are provided for the six subjects for data sets A and B, right (d) and left (s) eyes, and retinal test locations; fixation or 0, 11, and 22° in the temporal retina. (−) Designations imply a steepening of the SCE-I function when taking the difference between the two measured functions; (+) values correspond to a flattening of the SCE-I function when making the same comparisons. The following tables show the differences in curvature between various test conditions. For example, post–pre gives the difference in curvature for the Stiles–Crawford function before patching and just after patch removal. A positive value of the difference implies that the quadratic fit has become flatter. For e.g. if $Abs(rho_{post}) < Abs(rho_{pre})$, then $-rho_{post} - (-rho_{pre}) = rho_{pre} - rho_{post}$ which is >0.

data sets and between different test loci at the 1% level, no significant difference between eyes even at the 5% level, and a difference between different test conditions at the 5% level and an almost significant difference at the 1% level. Looking at the difference in the least square means, the most significant contribution to this difference comes from the recovery and the pre-patch data and an almost significant contribution at the 5% level between the recovery and the post-patch data. The actual values of the least squares means indicate that the curvature has become steeper for the recovery data.

For Table 5, part 2, X_{max}, there is no significant difference across A and B data sets or from different test conditions. There is a significant difference between retinal test loci at the 1% level, and a significant difference at the 1% level from an eye*(retinal test locus) interaction. As can be seen, there is a significant difference across the eyes at the 5% level.

These analysis were repeated with rho and X_{max} weighted by the inverse value of their variances ob-

tained from their quadratic fits. These results made no fundamental change in the conclusions stated in the last two paragraphs.

This statistical analysis does not reveal any significant changes between different test conditions (pre-patch, post-patch and recovery), supporting previous studies (Applegate et al., 1986; Enoch et al., 1987).

We, therefore, concluded the changes we seek to determine might be very small in relationship to the measured variances. We argued that small but significant changes may be 'buried' in these data sets. If such is the case, it is necessary to analyze these data by using techniques such as counts and histograms. Such approaches reveal trends but not absolute quantities for possible changes revealed.

5. Statistical analysis II

The counts and histograms proved to be both inter-

esting and highly productive. Using data presented in Tables 3 and 4, counts revealed strong trends, and histograms of these findings provided additional features of these data sets. That which facilitated these analyses was the observation that with recovery, 'overshoot' effects were indeed very common!

That is, if with dark-patching the peak of the SCE-I shifted X mm nasal (or temporal), and with recovery, the peak of the SCE-I function passed through it is original locus in the entrance pupil of the eye (X_{max} (pre-patch)) and now moved to the opposite side of that maximum, temporal (or nasal), this is a corrective overshoot response. An undershoot approached the pre-dark-patch locus of the SCE-I maximum, but did not pass it (assume this also is largely a corrective response). Conversely, in some cases, the peak might

Fig. 1. These are sample data sets of measurements of the Stiles–Crawford effect of the first kind for subject b. SCE-I functions are presented in pairs for purposes of comparison of outcomes. Curves are limited to the central portion of each function and have been fitted by Stiles' second order equation. Derived SCE-I peaks (X_{max}), V and V, and confidence limits (95%) are indicated. The abscissas are expressed in mm in the entrance pupil of the eye, zero is the center of the eye pupil. The ordinates, log relative directional sensitivity, are expressed in $\log_{10} \eta/\eta_{max} +$ (approximately) 1.0 log unit. That is, peaks of the individual SCE-I functions approximate a $\log_{10}$ value $= +1.0$ (see text and Table 2). In each figure, seeing to just non-seeing data (data set A, top set of curves) and non-seeing to just seeing (data set B, bottom set of curves) are presented for the same test conditions.
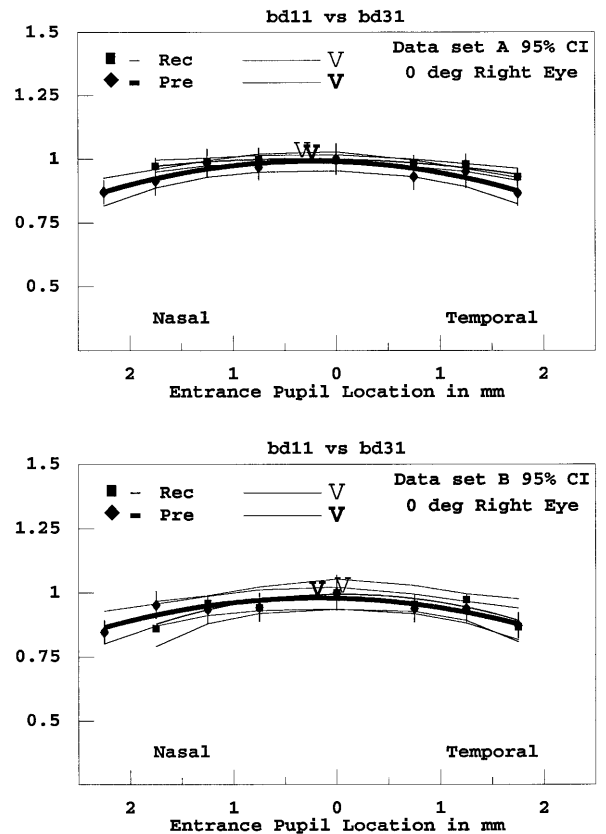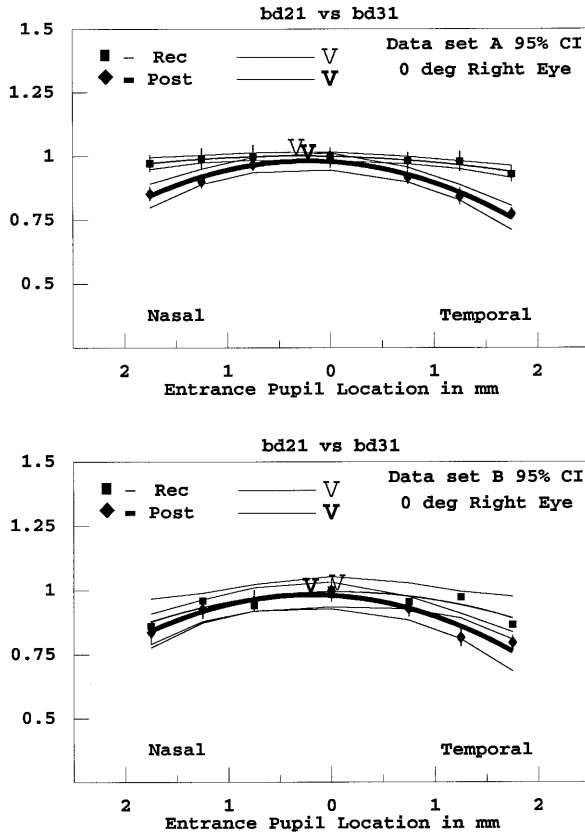

Fig. 2. These are sample data sets of measurements of the Stiles–Crawford effect of the first kind for subject b. SCE-I functions are presented in pairs for purposes of comparison of outcomes. Curves are limited to the central portion of each function and have been fitted by Stiles' second order equation. Derived SCE-I peaks (X_{max}), V and V, and confidence limits (95%) are indicated. The abscissas are expressed in mm in the entrance pupil of the eye, zero is the center of the eye pupil. The ordinates, log relative directional sensitivity, are expressed in $\log_{10} \eta/\eta_{max} +$ (approximately) 1.0 log unit. That is, peaks of the individual SCE-I functions approximate a $\log_{10}$ value $= +1.0$ (see text and Table 2). In each figure, seeing to just non-seeing data (data set A, top set of curves) and non-seeing to just seeing (data set B, bottom set of curves) are presented for the same test conditions.

shift further from the pre-dark-patch SCE-I X_{max} locus (also termed, 'more-of the same' -this is not a corrective response). In no case was there an exact match of the original locus pre-patch.

The same argument, overshoot, undershoot, and more of the same, applies to rho, i.e. the SCE-I parabola might become more curved or steeper (an increase in ρ), or the parabola might become more less curved or flatter.

Please refer to Table 3, which addresses differences in X_{max} values for an example of these counts. Refer to data A right eye (top data block), and compare difference values for post–pre with rec–post. At 0°, subject 'b' shows a corrective overshoot, T to N; subject 'e' a corrective overshoot T to N; 'k' a corrective overshoot N to T; 'v' a corrective overshoot N to T; 'p' a 'more

Fig. 3. These are sample data sets of measurements of the Stiles–Crawford effect of the first kind for subject b. SCE-I functions are presented in pairs for purposes of comparison of outcomes. Curves are limited to the central portion of each function and have been fitted by Stiles' second order equation. Derived SCE-I peaks (X_{max}), V and V, and confidence limits (95%) are indicated. The abscissas are expressed in mm in the entrance pupil of the eye, zero is the center of the eye pupil. The ordinates, log relative directional sensitivity, are expressed in $\log_{10} \eta/\eta_{max} +$ (approximately) 1.0 log unit. That is, peaks of the individual SCE-I functions approximate a $\log_{10}$ value $= + 1.0$ (see text and Table 2). In each figure, seeing to just non-seeing data (data set A, top set of curves) and non-seeing to just seeing data (data set B, bottom set of curves) are presented for the same test conditions.

Table 5
Statistical analyses: tests of fixed effects

| Source	Type III F	$Pr > F$
(Part 1) Test of fixed effects for rho or curvature of the parabola		
Eye	7.69	0.0694
Test conditions	5.74	0.0118
A and B data sets	36.96	0.0001
Retinal test locus	15.87	0.0001
(Part 2) Test of fixed effects for the peak of the SCE-I functions or X_{max}		
Eye	15.73	0.0286
Test conditions	0.62	0.5504
A and B data sets	0.02	0.8936
Retinal test locus	27.31	0.0001
Eye*retinal test locus	6.08	0.0031
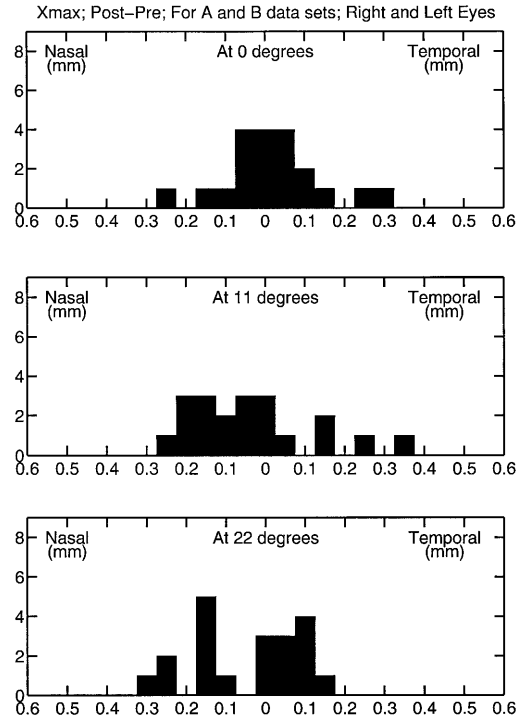
Fig. 4. These are histograms of X_{max} values for each of the three measured differences in results for the following pairs of test conditions, post–pre, rec–pre, and rec–post. Subjects, eyes, and data sets A and B have been combined. The ordinate is a count of X_{max} values recorded at designated mm differences, nasal and temporal on the abscissas. These same data are expressed in a different manner in Tables 3 and 4.

of the same'; 'w' a corrective undershoot. Thus, in this one sub-set of data there are four overshoots, one undershoot, and one 'more of the same'. Using the same subjects, referring to the same data block, at retinal test locus 11°, there are four overshoots (different individuals involved), and two undershoots, etc. For X_{max}, the magnitudes of changes encountered in Table 3 are plotted in histograms in Figs. 4–6. Sums of the types just tallied appear in Table 4, and for rho values the same sorts of counts are found in Table 6 (with histograms appearing in Figs. 7–9).

5.1. Such arguments led to an interesting set of conclusions/hypotheses

1. We postulated, that if curvature/rho changes occurred during dark patching, and those changes were restored during some time period after the dark-patch is removed, the largely corrective overshoot effect that we observed could explain the significant difference in the curvature between the recovery and the pre-dark-patch data and the smaller difference between the recovery and the post-dark-patch data. A count shows this effect to

be the most significant result in these experiments! In effect, this implies that photoreceptor alignment changes did occur during dark-patching. These were not picked up in the statistics, but are effectively revealed by the counted corrective overshoot effects (see Tables 6 and 7).

2. Similarly, it is possible to postulate, that while the statistical analysis does not reveal significant changes in X_{max} due to different test conditions, the trend analysis does suggest a powerful overshoot tendency with recovery in the direction of (and past) the initial measured SCE-I peak condition. This implies that the dark patching did, in fact, induce changes in X_{max} (see Table 6).

5.2. Analyses based on the histograms displayed in Figs. 4–9

The following analyses were conducted by taking simple averages of the differences of X_{max} over fixed variables such as eyes, A or B data sets and retinal test loci, and random variables such as subjects both with and without weights. The ratios of the means to their respective standard errors provide the z value, which then gives us a corresponding probability. The follow-
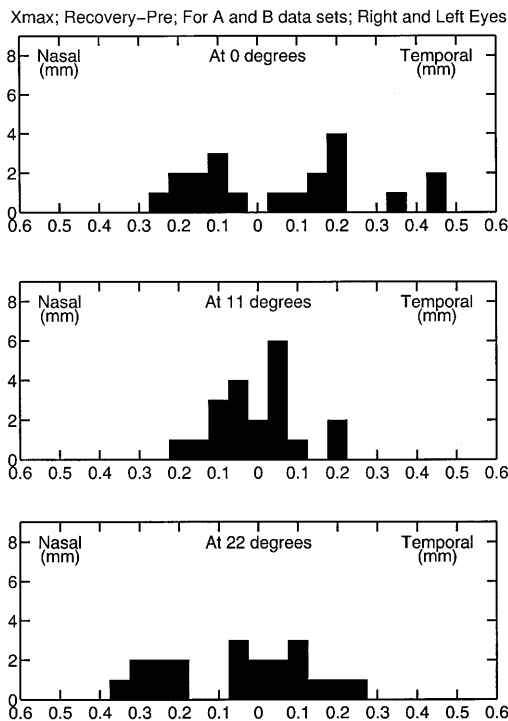

Fig. 5. These are histograms of X_{max} values for each of the three measured differences in results for the following pairs of test conditions, post–pre, rec–pre, and rec–post. Subjects, eyes, and data sets A and B have been combined. The ordinate is a count of X_{max} values recorded at designated mm differences, nasal and temporal on the abscissas. These same data are expressed in a different manner in Tables 3 and 4.
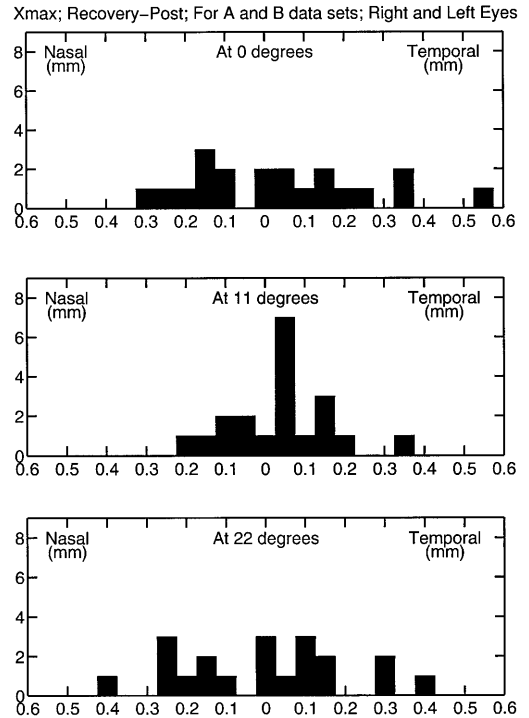

Fig. 6. These are histograms of X_{max} values for each of the three measured differences in results for the following pairs of test conditions, post–pre, rec–pre, and rec–post. Subjects, eyes, and data sets A and B have been combined. The ordinate is a count of X_{max} values recorded at designated mm differences, nasal and temporal on the abscissas. These same data are expressed in a different manner in Tables 3 and 4.

Table 6
Comparisons (1) recovery — post-patch test data versus (2) post-patch test data- pre-test data peak of the SCE-I function (location of X_{max})[a]

Angle	Number of estimates				
	#	&	@		Total estimates (R and L)
0°	13	1	6	=	20
11°	15	3	2	=	20
22°	14	4	2	=	20
Totals	42	8	10	=	60 Independent estimates

[a] #, Corrective overshoots with recovery in peak location opposite in direction to changes which took place during patching (N or T). &, Corrective undershoots with recovery in peak location opposite in direction to changes, which took place during patching (N or T). @, Increase in displacement of SCE-I peak in the same direction as noted during dark patching ('more of the same'). Total, changes during recovery of SCE-I peak location *which were opposite in direction* to changes occurring during patching, $42 + 8 = 50$ of 60 independent estimates (88 of 100%).

ing tables list probability values for the reliability of the means of differences for the several test conditions and at different test loci. These probability values are calculated assuming that the distribution of the differences for X_{max} follows a normal distribution. As seen from

the histograms in Figs. 4 and 5 and Table 6, this is not strictly a valid assumption. However, these are very valuable forms of analyses.

The calculations in Table 8 are performed with the data sets weighted by the inverse of the variance obtained for X_{max} from the quadratic fits. As seen from Table 8a, there is no significant difference in the means between the different test conditions at the 1% level at any of the test loci. However, there is a significant difference at 11° for the post–pre test condition at the 5% level. If these differences are averaged over all test loci, Fig. 8b shows a significant difference at the 1% level for the post–pre test condition, indicating that, the mean value X_{max} has indeed moved nasally by approximately 0.04 mm after patching as seen from Fig. 8c. The SCE-I peak, X_{max}, is seen to move temporally when the test is performed a few days after patch removal, although the reliability of this conclusion can be questioned at the 5% level.

Most important, 88% of these data sets show a trend towards their original pre-test setting. Of that sum, approximately 67% of these data sets represented cor-
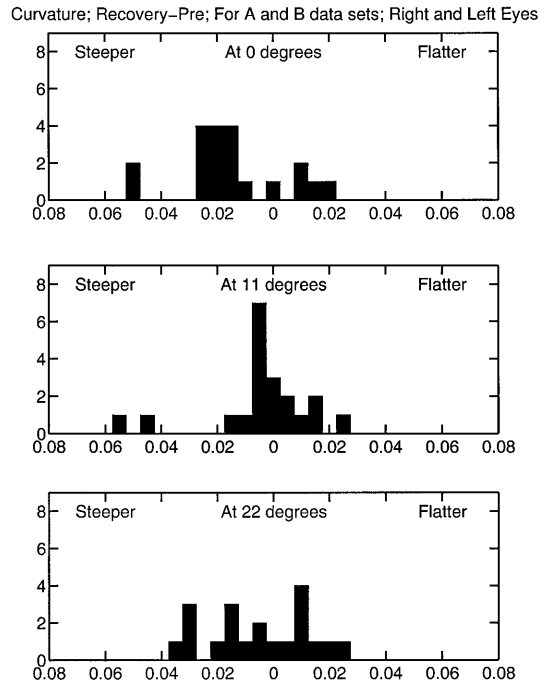

Fig. 7. These are histograms of $\Delta\rho$ values for each of the three measured differences in results for the following pairs of test conditions, post–pre, rec–pre, and rec–post. Subjects, eyes, and data sets A and B have been combined. The ordinates provide a recorded count of $\Delta\rho$ values. Negative values of $\Delta\rho$ on the abscissas indicate an increase in curvature of the parabola, and positive values indicate a flattening of the parabola in the comparisons of data samples. Rho (ρ) is a non-linear relationship, but because the range of differences in $\Delta\rho$ is small, the non-linear effects are modest. These same data are expressed in a different manner in Tables 4 and 7.
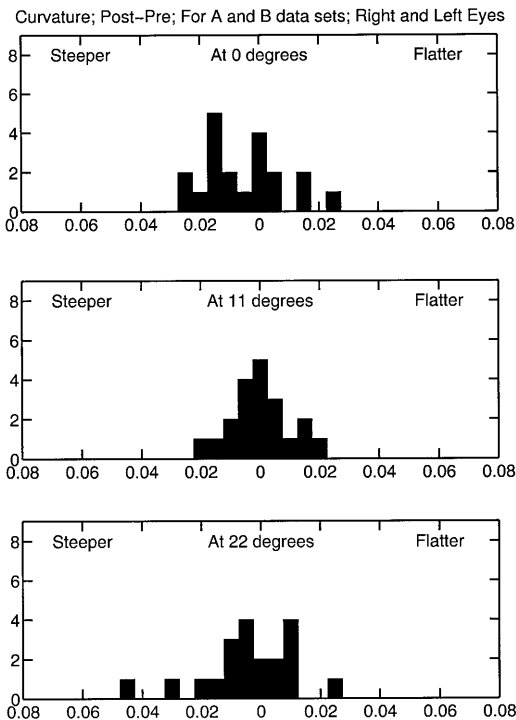

Fig. 8. These are histograms of $\Delta\rho$ values for each of the three measured differences in results for the following pairs of test conditions, post–pre, rec–pre, and rec–post. Subjects, eyes, and data sets A and B have been combined. The ordinates provide a recorded count of $\Delta\rho$ values. Negative values of $\Delta\rho$ on the abscissas indicate an increase in curvature of the parabola, and positive values indicate a flattening of the parabola in the comparisons of data samples. Rho (ρ) is a non-linear relationship, but because the range of differences in $\Delta\rho$ is small, the non-linear effects are modest. These same data are expressed in a different manner in Tables 4 and 7.

rective overshoots. Note that shifts in directions of these overshoots can be in either direction, nasal or temporal!

The calculations in Table 9 have been obtained without weighting X_{max}. Examining Fig. 9a, as before, we see that there are no significant differences in the means between different test conditions at any test locus at the 5% level. Furthermore, there is no significant effect between any test condition at the 5%, summing over all test loci. This result is not surprising in view of the fact, that previously, we were biasing in favor of the better fitted data. However, we see that X_{max} has still shifted nasally after patching by about 0.02 mm., and testing a few days after patch removal shifts X_{max} temporally, as seen before in Fig. 8a–c.

When assessing the latter set of statistical analyses (Statistical Analyses II), it should be remembered that we have pooled eyes as well as A and B data sets, and have counted all changes, e.g. recovery–post-dark-patching, and recovery–pre-dark-patching nasal to temporal and temporal to nasal as overshoots. A similar, if slightly different statement, might be said of trends in undershoots, and 'more of the same'. Ditto for ρ estimates, steeper to flatter and flatter to steeper.

Both types of changes have been considered as overshoots in recovery-post and recovery-pre assessments etc.
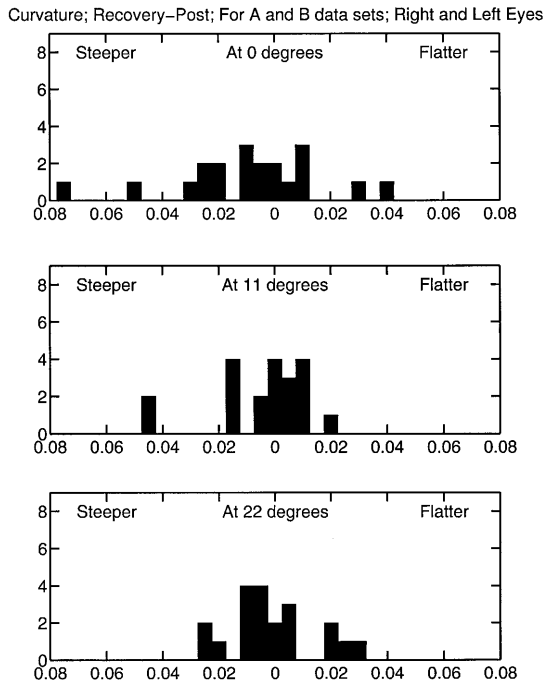

Fig. 9. These are histograms of $\Delta\rho$ values for each of the three measured differences in results for the following pairs of test conditions, post–pre, rec–pre, and rec–post. Subjects, eyes, and data sets A and B have been combined. The ordinates provide a recorded count of $\Delta\rho$ values. Negative values of $\Delta\rho$ on the abscissas indicate an increase in curvature of the parabola, and positive values indicate a flattening of the parabola in the comparisons of data samples. Rho (ρ) is a non-linear relationship, but because the range of differences in $\Delta\rho$ is small, the non-linear effects are modest. These same data are expressed in a different manner in Tables 4 and 7.

Table 7
Comparisons (1) recovery–post-patch test data vs. (2) post-patch test data — pre-test data curvature of the SCE-I parabolic function (Stiles' rho)[a]

Angle	Number of estimates				
	#	&	@		Total estimates (R and L)
0°	10	5	5	=	20
11°	12	4	4	=	20
22°	9	6	5	=	20
Totals	31	15	14	=	60 Independent estimates

[a] #, Corrective overshoots in curvature with recovery in the direction opposite to changes which took place during patching (steeper of flatter). &, Corrective undershoots in curvature with recovery in the direction opposite to changes which took place during patching (steeper of flatter). @, Increase in curvature of SCE-I function in the same direction (steeper or flatter) noted during patching ('more of the same'). Total, changes during recovery in curvature (rho) *opposite in direction* to changes occurring during patching, $31 + 15 = 46$ of 60 independent estimates (77 of 100%).

6. Statistical analysis III

The data were analyzed as a tri-level split-plot design with repeated measures at the lowest split level using Proc Mixed of SAS (Littell et al., 1996). Two different statistical models were used (see URL for reasons of brevity).

The results basically show that.

1. There are no significant difference between the test conditions (pre-patch, post-patch) for X at the 1 and 5% significance level at any of the test loci. However, it is seen that X_{max} has shifted nasally after patching by about 0.02 mm, and testing a few days after patch removal shifts X_{max} temporally.
2. There are no significant differences between post- and pre-patch results for the curvature at both the 5 and 1% significant level.
3. With regard to the post-patch versus recovery data, we find that it seems to be almost significant at the 5% level. However, the contribution that is really significant is the pre-patch versus recovery data. These results are significant at even the 1% level. In fact, it appears as though the curvature becomes steeper at recovery.
4. Approximately 88% of the data sets show a trend of movement of X_{max} post-patch toward the original pre-test value. Of that sum, approximately two thirds of these data set represented overshoots. We wish to underscore the point that even though the statistical analysis did not reveal any significant changes in X_{max} due to different test conditions, the overshoots suggest that dark patching did induce changes in X_{max}.

7. Discussion and conclusions

SCE-I changes recorded with dark-patching in normal eyes are very small, and hence earlier attempts to define these events did not reveal them (Enoch et al., 1980 Applegate et al., 1986).

The key to analysis of these data is found in the measured, largely corrective, overshoots recorded with recovery. This finding was unexpected. Yet, if changes had not occurred during dark-patching, why would the powerful phototropic mechanism exhibit largely corrective over-compensations when the dark-patch was finally removed after eight days? Also, this provides interesting information about the nature of the phototropic feedback mechanism. The reader is urged to study carefully Tables 3, 4, 6 and 7, which are counts derived directly from the former two tables. Similarly, the histograms (Figs. 4–9) provide valuable additional information.

While Fig. 4 and some aspects of these analyses hint at support for the working hypothesis, that conclusion

Table 8
Statistical analyses of X_{max} using counts and histograms (with weights)

Retinal test Locus	Post–pre (Δmm)	Recovery–pre (Δmm)	Recovery-post (Δmm)
(a) Probability values for the reliability of the difference in means for X_{max} for the following sets of test conditions, (with weights obtained from the quadratic fits			
0°	0.3977	0.2661	0.0973
11°	0.0325	0.1626	0.1582
22°	0.1435	0.2613	0.3980
(b) Probability values for the reliability of the difference in means for X_{max} for the following sets of test conditions for all test loci combined, (with weights obtained from the quadratic fits)			
	0.0101	0.2299	0.1276
(c) Difference in means for X_{max} (in mm) for the following sets of test conditions for all test loci combined, (with weights obtained from the quadratic fits)			
	0.0393 N	0.0184 N	0.0274 T

Table 9
Statistical analyses of X_{max} using counts and histograms (without weights)

Retinal test locus	Post–pre (Δmm)	Recovery–pre (Δmm)	Recovery–post (Δmm)
(a) Probability values for the reliability of the difference in means for X_{max} for the following sets of test conditions (without weights obtained from quadratic fits)			
0°	0.3230	0.1826	0.2920
11°	0.2637	0.3951	0.1736
22°	0.1238	0.1872	0.3984
(b) Probability values for the reliability of the difference in means for X_{max} for the following sets of test conditions for all test loci combines. (without weights obtained from the quadratic fits)			
	0.2131	0.3932	0.2420
(c) Difference in means for X_{max} (in mm) for the following sets of test conditions for all test loci combined, (without weights obtained from the quadratic fits)			
	0.0210 N	0.0037 T	0.0247 T

is not convincing. Rather, the results suggest that small changes do occur in receptor alignments in the dark, that these may alter SCE-I peak alignments locally either nasally or temporally (and one supposes superiorly or inferiorly), and that these changes may result in increases or decreases in curvature of the SCE-I function. In short, if one avoids major tractional events or their sequelae (as was done here), we are looking at multiple mechanisms of limited strength exerting strains upon the retina, and these vary from person-to-person, eye-to-eye, and location-to-location (and possibly from time-to-time). And they may not be uniform across the retina. Thus, the need to test multiple retinal loci when assessing photo-receptor alignments.

The latter statements do not explain the sub-set of eyes, discussed above, where center-of-the-retinal-sphere pointing is encountered, nor do they explain modest nasal biases recorded repeatedly in many SCE-I studies.

This study helps explain why few changes in receptor alignments occur overnight or during sleep (critical for species survival), or during short-term eye patching, e.g. as used clinically for various purposes. So long as the dominant phototropic mechanism is active, there is no

reason for there to be a diminution or major change in the SCE-I with time or aging. Remarkable SCE-I peak location stability with aging has been found in most all normal observers tested to date (e.g. see Rynders et al., 1995).

Thus, there are apparent rather small changes in alignment of photoreceptors in the dark, these are not of a predictable nature (possibly because we are dealing with multiple competing mechanisms). In normal eyes, these are readily over-ridden by the dominant phototropic alignment mechanism, which exhibits a largely corrective overshoot tendency during recovery. We wish that these effects were more easily defined and revealed.

Clearly, further studies of these effects are indicated, and longer periods of recovery need to be utilized. Perhaps techniques in development for fine assessment of retinal images in living human eyes and advanced aberration controls can be used to further our understanding of transients in photoreceptor alignments (e.g. see several articles in Lakshminarayanan, 1997, including studies by Williams, Liang, Miller, Roorda, Packer, M. Campbell, Glasser, Roorda, & Williams, 2000; Smallman, Fine, & MacLeod, 2000). Methods employed for following transient-induced changes could

be similar to those used by Zwick et al. (1997, 1999) in snake eyes. Obviously, in this case, techniques for inducing receptor orientation transients other than laser burns would have to be employed. Finally, small changes measured in the SCE-I in pupillary space can represent meaningful events are occurring at the retina.

Acknowledgements

Appendix A. Curve fitting of directional sensitivity data using Stiles' formula

1. By limiting analysis to the central portion of the measured SCE-I function (2.5–3.0 mm from X_{max}), a parabola adequately fits these data (e.g. Stiles, 1937; Enoch & Tobey, 1981; Enoch & Lakshminarayanan 1991; Lakshminarayanan & Enoch, 1985).

2. In the eye pupil, the 'true center' of the determined SCE-I paraboloid of rotation may not pass through the center of the entrance pupil. Importantly, when employing a parabolic fitting procedure, an estimate of curvature computed with Stiles' ρ function is not affected by such a displacement or error (Stiles, 1937; Lakshminarayanan and Enoch, 1985).

3. Log relative directional sensitivity, $\log_{10} \dot{\eta}/\dot{\eta}_{max}$, is described as follows (Stiles, 1937):

$$\frac{\eta'}{\eta'_{max}} = 10^{\{-\rho|X-X_{max}|^2\}} \log_{10} \frac{\eta'}{\eta'_{max}} = -\rho|X-X_{max}|^2;$$

where η' is the retinal directional sensitivity measured at the test locus; η'_{max} the retinal directional sensitivity at the maximum of sensitivity in the pupil meridian tested; X the lineal displacement in the entrance pupil of the eye, in mm, from the peak of directional sensitivity in the meridian tested; and X_{max} is the location of the peak of directional sensitivity in the (in this case) horizontal meridian tested in the entrance pupil of the eye.

For plotting log relative sensitivity (ordinate) values on graphs, all values were multiplied by $10 \times$, so that maxima of SCE-I curves are plotted at $\log_{10} \dot{\eta}/\dot{\eta}' = 1.0$. In tables and figures which follow, and others which are contained in the URL (see below), the adjustment for normalcy of $\dot{\eta}/\dot{\eta}'$ at X_{max} did not quite equal 1.0; this was later corrected later in statistical analyses.

References

Applegate, R. A., & Bonds, A. B. (1981). Induced movement of receptor alignment toward a new pupillary aperture. *Investigative Ophthalmology and Visual Science*, *21*, 869–873.

Applegate, R. A., Adams, A. J., Bradley, A., & Eisner, A. (1986). Total occlusion does not disrupt photoreceptor alignment. *Investigative Ophthalmology and Visual Science*, *27*, 441–443.

Bedell, H. E., & Enoch, J. M. (1980). An apparent failure of the photoreceptor alignment mechanism in a human observer. *Archives of Ophthalmology*, *98*, 2023–2026.

Bonds, A. B., & MacLeod, D. I. A. (1978). A displaced Stiles–Crawford effect associated with an eccentric pupil. *Investigative Ophthalmology and Visual Science*, *17*, 754–761.

Campos, E. C., Bedell, H. E., Enoch, J. M., & Fitzgerald, C. R. (1978). Retinal receptive field-like properties and Stiles–Crawford effect in a patient with a traumatic choroidal rupture. *Documenta Ophthalmologica*, *45*, 381–395.

Chaitin, M. H., & Burnside, B. (1989). Actin filament polarity at the site of rod outer segment disk morphogenisis. *Investigative Ophthalmology and Visual Science*, *30*, 2461–2469.

Enoch, J. M. (1972a). Retinal receptor orientation and the role of fiber optics in vision. *American Journal of Optom and Arch American Acad Optom*, *49*, 455–470.

Enoch, J. M. (1972b). The two-color threshold technique of Stiles and derived component color mechanisms, chapter in the Psychophysics section. In L. Hurvich, *The handbook of sensory physiology*, vol. VII/4. New York: Springer A secondary source with multiple references and a description of the techniques employed.

Enoch, J. M., & Birch, D. (1981). Inferred positive phototropic activity in human photoreceptors. *Phil Transactions Royal Society of London*, *291*(B1051), 323–351.

Enoch, J. M., & Birch, D. G. (1985). Comment on inferred positive phototropic activity in human photoreceptors. *Phil Transactions Royal Society of London*, *B309*, 611–613.

Enoch, J. M., & Hope, G. M. (1972). An analysis of retinal receptor orientation: III. Results of initial psychophysical tests. *Investigative Ophthalmology*, *11*, 765–782.

Enoch, J. M., & Lakshminarayanan, V. (1991). Retinal fibre optics. In W. N. Charman, *Vision and visual dysfunction, visual optics and instrumentation*, vol. 1 (pp. 280–309). London: Macmillan Books.

Enoch, J. M., & Stiles, W. S. (1961). The color change of monochromatic light with retinal angle of incidence. *Optica Acta*, *8*, 329–358.

Enoch, J. M., & Tobey, F. L. (1981). Vertebrate photoreceptor optics. In *Springer series in optical sciences*, vol. 23. Heidelberg: Springer.

Enoch, J. M., Birch, D. G., & Birch, E. E. (1979). Monocular light exclusion for a period of days reduces directional sensitivity of the human retina. *Science*, *206*, 705–707.

Enoch, J. M., Birch, D. G., Birch, E. E., & Benedetto, D. D. (1980). Alteration in directional sensitivity of the retina by monocular occlusion. *Vision Research*, *20*, 1185–1189.

Enoch, J. M., Eisner, A., & Bedell, H. E. (1982). Further evaluation of an apparent failure of the photoreceptor alignment mechanism in a human observer. *Archives of Ophthalmology*, *100*, 1280–1281.

Enoch, J. M., Hamer, R. D., Lakshminarayanan, V., Yasuma, T., Birch, D. G., & Yamade, S. (1987). Effect of monocular light exclusion on the Stiles–Crawford function. *Vision Research*, *27*, 507–510.

Enoch, J. M., Lakshminarayanan, V., & Yamade, S. (1986). The Stiles–Crawford effect (SCE) of the first kind: studies of the SCE in an aniridic observer. *Perception*, *15*, 777–784.

Lakshminarayanan, V., Enoch, J. M., & Yamade, S. (1987). In A. Fiorentini, D. L. Guyton, & I. M. Siegel, *Human photoreceptor orientation: normals and exceptions. Advances in diagnostic visual optics* (pp. 28–32). Heidelberg: Springer.

Lakshminarayanan, V., & Enoch, J. M. (1985). Shape of the Stiles–Crawford function for traverses of the entrance pupil not passing through the peak of sensitivity. *American Journal of Optom Physics Optics*, *62*, 127–128.

Lakshminarayanan, V., Enoch, J. M., & Yamade, S. (1987). In A. Fiorentini, D. L. Guyton, & I. M. Siegel, *Human photoreceptor orientation: normals and exceptions. Advances in diagnostic visual optics* (pp. 28–32). Heidelberg: Springer.

Littell, R. C., Milliken, G. A., Stroup, W. W., & Wolfinger, R. D. (1996). *SAS system for mixed models*. Cary, NC: SAS Institute Inc.

Roorda, A., & Williams, D. R. (2000). Angular tuning of single cones in the living eye. *Investigative Opthalmology and Vision Science*, *41*(4), S100.

Rynders, M., Grosvenor, T., & Enoch, J. M. (1995). Stability of the Stiles–Crawford function in a unilateral amblyopic subject over a 38 year period: a case study. *Optometry and Vision Science*, *72*(3), 177–185 this paper contains a list of reports which address the stability of SCE-I over time. Recently, DeLint PJ, Vos JJ, Berendschot T, Van Norren D. On the Stiles–Crawford effect with age. Investigative Ophthalmology and Visual Science 1997; 38 (6): 1271–1274, added new data to this topic.

Smallman, H. S., Fine, I., & MacLeod, D. I. A. (2000). Visual processing before and after removal of bilateral congenital cataracts in adulthood: receptor reorientation and visual suppression. *Investigative Ophthalmology and Visual Science*, *41*(4), S100.

Stiles, W. S. (1937). The luminous efficiency of monochromatic rays entering the eye pupil at different points and a new color effect. *Proceedings of the Royal Society of London*, *B123*, 90–118.

Stiles, W. S., & Crawford, B. H. (1933). The luminous efficiency of rays entering the eye pupil at different points. *Proceedings of the Royal Society of London*, *B112*, 428–450.

Westheimer, G. (1969). Personal communication, re: the need to re-evaluate eye movement factors associated with determinations of SCE-I. December 1998. *Journal of Optical Society of America*, *59*, 617–623 This discussion refers to earlier studies by W. Richards.

Zwick, H., Elliott, R., Schuschereba, S. T., Lund, D. J., & Stuck, B. E. (1997). In vivo scanning laser ophthalmoscopic characterization of retinal pathology in a small eye animal model. In B. E. Stuck, & M. Belkin, *Laser and noncoherent ocular effects: epidemiology, prevention, and treatment*, vol. 2974 (pp. 44–49). SPIE.

Zwick, H., Elliott, R., Li, G., Akers, A., Edsall, P. R., & Stuck, B. E. (1999). In B. E. Stuck, & M. Belkin, *In vivo imaging of photoreceptor structure and laser pathophysiology in the snake eye*, vol. 3591 (pp. 368–374). SPIE.